Measurement of CO_2 isotopologue ratios using a hollow-waveguide based mid-infrared dispersion spectrometer

Haojie Zhang,[†] Tao Wu, *,[†] Qiang Wu,[‡,†] Weidong Chen,[§] Chenwen Ye,[†] Mengyu Wang,[†] Xingdao He[†]

[†]Key Laboratory of Nondestructive Test (Ministry of Education), Nanchang Hangkong University, Nanchang, 330063, China

[‡]Department of Mathematics, Physics and Electrical Engineering, Northumbria University, Newcastle upon Tyne, NE1 8ST, UK

[§]Laboratoire de Physicochimie de l'Atmosphère,Université du Littoral Côte d'Opale 189A, Av. Maurice Schumann, Dunkerque 59140, France

*E-mail: wutccnu@nchu.edu.cn

ABSTRACT: We demonstrate for the first time the measurement of CO_2 isotope ratios ($^{13}C/^{12}C$ and $^{18}O/^{16}O$) in a hollow waveguide (HWG) fiber using a mid-infrared heterodyne phase-sensitive dispersion spectrometer (HPSDS). A 4.329 μm interband cascade laser (ICL) is used to target the absorption lines of three CO_2 isotopes ($^{13}C^{16}O_2$, $^{18}O^{12}C^{16}O$, and $^{12}C^{16}O_2$) in a 1 m long and 1 mm inner diameter HWG fiber. The detection limits are 0.29 ppm, 65.78 ppb and 14.65 ppm with an integration time of 218 s for $^{13}C^{16}O_2$, $^{18}O^{12}C^{16}O$, and $^{12}C^{16}O_2$, respectively, at a modulation frequency of 160 MHz and a pressure of 230 mbar. The measurement precisions of $\delta^{13}C$ and $\delta^{18}O$ are 0.89 ‰ and 0.88 ‰, respectively, corresponding to an integration time of 167 s. An experimental comparison between a HPSDS and a built wavelength modulation system with second-harmonic detection (WMS-2f) is conducted. The results show that compared to the WMS-2f, the developed HPSDS exhibits a greater linear dynamic range and excellent long-term stability. This work aims to demonstrate a detection technique of CO_2 isotope dispersion spectroscopy with a large dynamic range for relevant applications focusing on samples with high concentrations of CO_2 (% volume fraction), such as respiratory analysis in medical diagnostics.

Carbon and oxygen isotope analysis of carbon dioxide (CO_2) is widely used in geochemistry, atmospheric chemistry and medical diagnostics [1-4]. In geochemistry, quantification of $^{13}C/^{12}C$ isotope ratios in volcanic CO_2 gas is helpful for understanding changes in source regions, and volcanic activity monitoring. Measurement accuracy of $\delta^{13}C$ with 0.5‰ or better is important for a deeper understanding of volcanic system formation [5]. In atmospheric chemistry, ^{13}C and ^{18}O serve as tracers that can accurately track and predict changes in CO_2 concentrations to determine the distribution of carbon sources and sinks in nature [6]. Precision in the range of 0.01 to 0.3‰ is of interest in atmospheric chemistry. In the medical field, as established molecular biomarkers, changes in the contents of $^{13}CO_2$, $^{18}O^{12}C^{16}O$ and $^{12}CO_2$ in exhaled breath can be used to monitor multiple disease patterns, such as the diagnosis of Helicobacter pylori infections and non-invasive monitoring of glucose metabolism [7-8]. In the ^{13}C-urea breath test (UBT), the delta over baseline (DOB) value relative to standards can be used to demonstrate the enrichment of ^{13}C [9]. ^{18}O isotope analysis in breath gas can also be used to assist in the diagnosis of Helicobacter pylori pathogenesis [10]. A short-term precision of 0.5-1 ‰ for $\delta^{13}C$ and $\delta^{18}O$ determination is usually required for practical clinical applications [11].

Isotope ratio mass spectrometry (IRMS) [12], non-dispersive isotope selective infrared spectroscopy (NDIRS) [13] and laser absorption spectroscopy (LAS) [14] techniques are established as routine techniques for stable isotope analysis. IRMS demonstrates excellent quality in terms of precision and accuracy, but it also has drawbacks such as sample pretreatment, large space occupation, high instrument cost, and the need for professional operation and maintenance. The NDIRS shows similar precision as the IRMS and provides a simpler instrument setup. However, commercial instruments typically do not support simultaneous multi-component analysis and a rather large sample volume (over 100 ml) is required. Compared to IRMS and NDIRS, LAS technology [15-19] has received increasing attention owing to its advantages such as high selectivity, fast response, small instrument size, simple operation, real-time online analysis, and the ability to determine multiple analytes simultaneously. In recent years, various techniques based on LAS for measuring carbon isotope ratios have been investigated, including off-axis integral cavity spectroscopy (OA-ICOS) [20], cavity ring-down spectroscopy (CRDS) [21], and wavelength modulation spectroscopy (WMS) [22]. LAS-based detection instruments have been demonstrated for CO_2 isotope ratio measurements in mouse breath or human breath (CO_2 concentrations from 2% up to 5%). Tütüncü *et al.* [23] used balanced detection in a miniature dual-channel substrate-integrated hollow waveguide to monitor $^{13}CO_2$ enrichment levels in mouse breath samples based on mid-infrared absorption spectroscopy. The reported sensor has a $\delta^{13}C$ accuracy of 1.3‰ over an integration time of 480 seconds, and demonstrating the feasibility of on-line analysis for exhaled breath isotopes in microliter gas samples. Zhou *et al.* [24] reported a gas sensor with mid-infrared HWG for measuring CO_2 isotopes in human exhaled gas through the calibration-free WMS. The precisions of

$\delta^{13}C$ and $\delta^{18}O$ obtained by the sensor were 0.26 ‰ and 0.57 ‰, respectively, within an integration time of 131 seconds. However, in most LAS techniques, the obtained signal amplitude is strongly dependent on the optical power level. Any additional losses and power fluctuations can have a significant impact on the performance of the sensing system. For example, in WMS, frequency shift of a free-running semiconductor laser under long-term operation without imposing additional frequency stabilization facilities is frequently found in the output spectra, which makes it challenging to achieve long-term system stability [25]. Furthermore, according to the Beer-Lambert law, it exists a non-linear relationship between the sample concentration and its absorption at high absorbance conditions [26].

In recent years, laser dispersion spectroscopy has received increasing attention in the field of gas sensing. Dispersion spectroscopy is used to study the properties of samples by measuring the differential phase of multiple light waves caused by abnormal refractive index changes in the vicinity of molecular resonances [27]. The refractive index function of dispersion is proportional to the sample concentration at the limitation of Kramers-Kronig law. As a result, compared to absorption-based measurement methods, dispersion spectroscopy has a greater linear dynamic range for measuring sample concentrations. Different detection schemes based on dispersion spectroscopy have been established, including frequency modulation spectroscopy (FMS) [28], frequency comb spectroscopy (FCS) [29], chirped laser dispersion spectroscopy (CLaDS) [30], and heterodyne phase-sensitive dispersion spectroscopy (HPSDS) [31]. FMS uses a high-speed phase modulator and a phase shifter to probe molecular absorption and dispersion. High modulation frequencies allow to lower 1/f laser amplitude noise. However, due to the fact that dispersion information is extracted from the amplitude of the output signal, this process is still very sensitive to power fluctuations. FCS can achieve high-precision and broadband simultaneous measurement of molecular absorption and dispersion. However, the cost and technical complexity of high-precision and stable frequency comb sources limit their further applications in the sensing field. As field-deployable gas detection technologies, both CLaDS and HPSDS are based on the high-frequency intensity modulation of the laser output to retrieve dispersion distributions [32-35]. Since the measured quantity is phase-shift independent of light intensity, they are not affected by fluctuations in laser power. Unlike CLaDS, which requires a high-performance real-time spectrometer to perform frequency demodulation of the beat signal and a more complex data acquisition system, HPSDS directly retrieves the phase of the down-converted beat signal through a lock-in amplifier [36-37]. In contrast to the CLaDS, HPSDS has a simpler optical setup and signal processing system. To the best of our knowledge, there are currently no literature reports on HWG-based HPSDS measurements of CO_2 isotopes.

The measurement of CO_2 isotope ratios has mainly focused on the spectral regions around 1.6 μm, 2.0 μm, and 4.3 μm [38-40]. The CO_2 molecular absorption line intensities in the 4.3 μm band are much higher than in the 1.6 μm and 2.0 μm bands and can be accessed by a compact mid-infrared interband cascade laser (ICL) or quantum cascade laser (QCL). Therefore, combining the greater linear dynamic range of HPSDS with the strong absorption line intensity of 4.3 μm, it is attractive to develop HPSDS-based gas sensors to measure CO2 isotopologues in the mid-infrared (MIR) spectral region. MIR HPSDS measurements are usually performed by modulating the injection current of a semiconductor laser at high frequencies ranging from 100 MHz to 2 GHz. Martin *et al.* [41] first demonstrated mid-infrared HPSDS by high-frequency modulation of a 4.58 μm QCL at 160 MHz to detect 3 ppm CO at 100 mbar. Ma *et al.* [42] applied HPSDS to combustion measurements based on a directly modulated ICL. Modulating the injection current of a semiconductor laser inevitably introduces synchronous intensity modulation (IM) and frequency modulation (FM) [43]. The existence of FM results in an asymmetrical signal line shape of HPSDS. Moreover, due to the out-of-phase of FM sidebands, a larger phase shift will be experienced in the center of the line, leading to an increase in the HPSDS peak and a decrease in the linear dynamic range [41].

Benefitting from the low sample volume (hundreds of μL) and low-loss optical transmission, the hollow waveguide fiber allows for a compact instrument design, fast response time, and appreciable sensitivity over short path lengths [44]. In this work, we report a combination of HPSDS technology and a low-volume HWG fiber to detect CO_2 isotopes. A 4.329 μm ICL is used as light source to target three absorption lines of CO_2 isotopes ($^{13}C^{16}O_2$, $^{18}O^{12}C^{16}O$, and $^{12}C^{16}O_2$). The performance at different pressures, modulation frequencies and modulation depths is investigated to optimize the system setup. The Allan variance is used to evaluate the long-term stability and the minimum detection limit of the sensor. Measurement precision of $\delta^{13}C$ and $\delta^{18}O$ is also determined. We also performed an experimental comparison of HPSDS and WMS-2f. The proposed sensing system is expected to be used for respiratory analysis.

The principle for HPSDS has been well documented in the previous research [43] and is only briefly described here. Molecular dispersion spectroscopy relies on detection of the phase signal associated with the variation of the refractive index in the vicinity of a molecular transition. This process is accompanied by gas absorption and can be correlated through the Kramers-Kronig relationship for the refractive index $n(\omega)$ and absorption coefficient $\alpha(\omega)$:[45]

$$n(\omega) = 1 + \frac{c}{\pi}\int_0^{+\infty} \frac{\alpha(\omega')}{\omega'^2 - \omega^2} d\omega' \quad (1)$$

where c is the speed of light in vacuum, ω is the optical angular frequency. Therefore, the dispersion distribution of the molecule can be retrieved from its absorption spectral line shape parameter.

Mid-infrared HPSDS is based on the emission of a three-tone laser beam consisting of a carrier (E_1) and two sidebands (E_2, E_3) by modulating the injection current of an ICL or a QCL at high frequencies (several hundred MHz or GHz), and subsequently accessing the dispersion information through their phase shift due to refractive index changes near the target molecular transition. It is noted that this modulation changes both the output optical frequency as well as the intensity introducing a mixed characteristic of intensity modulation (IM) and frequency modulation (FM). Also, this characteristic is affected by the tuning factor of the used semiconductor laser [46] i.e. IM index m, FM index β, FM-IM phase shift θ. In the vicinity of the target absorption line, each tone travels at different phase velocities senses, resulting in an optical phase shift

within these tones. When the three-tone beam impinges the (square law) detector, beat note signals are generated between the center carrier wave and the two sidebands, and its phase can be expressed as:

$$\varphi = \tan^{-1}\left\{\frac{\begin{array}{l}2A\beta\sin(\varphi_0-\varphi_1-\theta)-2B\beta\sin(\varphi_{-1}-\varphi_0-\theta)\\+Am\sin(\varphi_0-\varphi_1)+Bm\sin(\varphi_{-1}-\varphi_0)\end{array}}{\begin{array}{l}2A\beta\cos(\varphi_0-\varphi_1-\theta)-2B\beta\cos(\varphi_{-1}-\varphi_0-\theta)\\+Am\cos(\varphi_0-\varphi_1)+Bm\cos(\varphi_{-1}-\varphi_0)\end{array}}\right\} \quad (2)$$

The coefficient A = exp[-$\alpha(\omega+\Omega)L$-$\alpha(\omega)L$] and B = exp[-$\alpha(\omega-\Omega)L$-$\alpha(\omega)L$]. Where φ_0, φ_1 and φ_{-1} are the phases of the carrier wave E_0 and the two sidebands E_1 and E_{-1}, respectively, L is the absorption path length, Ω is the modulation frequency. The gas concentration can be thus determined from the phase of the beat note signal.

The $^{13}C/^{12}C$ and $^{18}O/^{16}O$ ratios in CO_2 are usually expressed as a deviation from the Vienna PDB (VPDB) standard, denoted as per mil (‰), the so-called δ-value:

$$\delta^{13}C = \delta^{13}C_{cal} + \frac{R_{sam}-R_{cal}}{{}^{13}R_{VPDB-CO_2}} \quad (3)$$

$$\delta^{18}O = \delta^{18}O_{cal} + \frac{R_{sam}-R_{cal}}{{}^{18}R_{VPDB-CO_2}} \quad (4)$$

where R_{sam} and R_{cal} are the measured ratios of $^{13}CO_2/^{12}CO_2$ and $^{18}O^{12}C^{16}O/^{12}CO_2$ for the sample gas and the calibration gas. $^{13}R_{VPDB\text{-}CO2}$ and $^{18}R_{VPDB\text{-}CO2}$ are the internationally recognized VPDB standards of 0.0110019 and 0.00411009, respectively [47].

EXPERIMENTAL SECTION

The experimental setup is shown in Figure 1. The HWG-based dispersion spectrum detection system for CO_2 isotopes is mainly composed of a laser, a 1 m long HWG fiber, a photodetector, and a modulation and demodulation system. The used laser is a 4.329 μm ICL from Nanoplus with a maximum output power of 12.5 mW. Its internal pump source and thermoelectric cooler (TEC) are integrated in a TO66 package with a collimating lens. The laser temperature and injection current are precisely controlled using a laser controller (LDC3724C, ILX Lightwave) with a current output accuracy of 0.05 % and a temperature control accuracy of ±0.1 °C. The central current and temperature of the ICL are set to 50.70 mA and 5.0 °C, respectively. A sawtooth signal with a repetitive frequency of 40 Hz and an amplitude of 550 mVpp generated by SG1 (DG822, RIGOL) is connected to the modulation input of the laser controller to scan absorption lines of $^{12}CO_2$, $^{13}CO_2$ and $^{18}O^{12}C^{16}O$. Due to the limited modulation bandwidth of the laser controller, a high-frequency signal (hundreds of MHz) cannot be directly fed into the laser through the laser controller. To perform HPSDS detection, we use an RF bias-tee circuit (ZFBT-6GW+, Minicircuits) to feed a 160 MHz high-frequency signal into the ICL to generate a three-tone beam. The DC port of the bias-tee circuit is used to access the bias current, and the AC port is used to access high-frequency signals of 160 MHz. The emitted three-tone beam is injected into the HWG (HWEA 10001600, Polymicro Technologies) fiber via a diaphragm. Here the diaphragm is used to filter part of the interfering optical signal. The three-tone laser beam carrying dispersion information transmitted from the HWG fiber is received by a photodetector (LABM-I-6, VIGO System) to generate a beat note signal at 160 MHz. Due to the relatively high frequency of the beat signals, commercial lock-in amplifiers cannot be used directly for detection. A sinusoidal signal at a frequency of 159.9 MHz generated from another channel of SG2 (DG4162, RIGOL) via PS2 is mixed with the detected beat signal in Mixer 2 to downshift the beat frequency of 160 MHz to 100 kHz. The reference signal of the lock-in amplifier is obtained from Mixer1 in the same way. The first harmonic phase information demodulated by the lock-in amplifier (SR830, Stanford Research Systems) is recorded with a data acquisition card and transmitted to a laptop for data processing.

The HWG fiber in this experiment has a length of 1 m, an inner diameter of 1 mm, and a volume of about 0.78 cm^3. Both ends of the fiber are fixed in an aluminum connector consisting of a gas connector, a CaF_2 wedge window piece, and an aluminum cap. The HWG was covered with silver foil, heater band, and insulation foam successively. A PID temperature controller and a platinum resistor embedded in the heating band maintain the temperature of the HWG fiber at 298.15 K with a controlled accuracy of 0.1 K. CO_2 samples at different standard concentrations used in the present experiment are obtained by diluting high-purity CO_2 with high-purity N_2. The dilution ratios are controlled using two mass flow controllers (CS200C, Sevenstar) at the inlet. The diluted CO_2 gas sample is pumped into the HWG via a 1.2 L/min diaphragm pump (1.2L DIVAC). A flow rate of 3.9 ml/s and an upstream pressure of 230 mbar within the HWG chamber are maintained by a pressure controller (IQP-600C, Bronkhorst), MFC3, and diaphragm pump. The excess mixture is released into the atmosphere via a tee-spilt and a balancing valve to equalize the pressure throughout the gas delivery system.

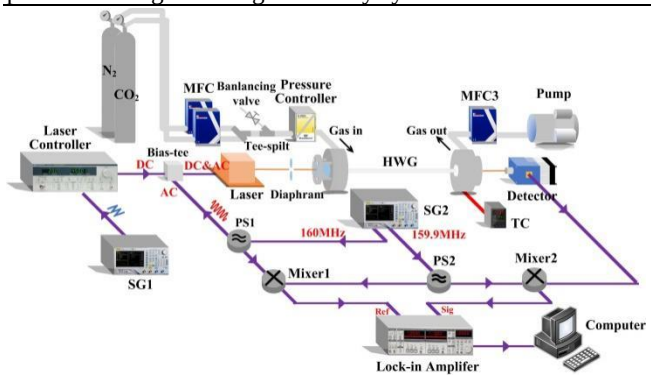

Figure 1. Schematic of the HWG-based experimental HPSDS setup for CO_2 isotopes measurements. SG1, SG2: signal generator; PS1, PS2: power splitter; TC: temperature controller; MFC: mass flow controller.

CO_2 isotopes have strong line intensities near 4.329 μm, which permits sensitive CO_2 isotope measurements in this spectral region. In this region, the absorption line intensities of the three isotopes $^{13}C^{16}O_2$, $^{12}C^{16}O_2$, and $^{18}O^{12}C^{16}O$ are all of the same order of magnitude (>10^{-21} cm^{-1}/ (molec·cm^{-2})), and the spectral-distances of the three absorption lines are within one wavelength scan of the available ICL. To avoid the interference of H_2O and its isotopic lines, Figure 2 shows a spectral simulation of 1% CO_2 and 1.2% H_2O for the spectral region from 2309.6 cm^{-1} to 2310.8 cm^{-1} at 298.15 K and 230 mbar with an absorption length of 1 m, based on the HITRAN2020 database [48]. $^{12}C^{16}O_2$ at 2310.002 cm^{-1}, $^{18}O^{12}C^{16}O$ at 2310.205

cm^{-1} and $^{13}C^{16}O_2$ at 2310.347 cm^{-1} are relatively well separated from each other [17], and there is no interference from the neighboring H_2O and its isotopic absorption lines.

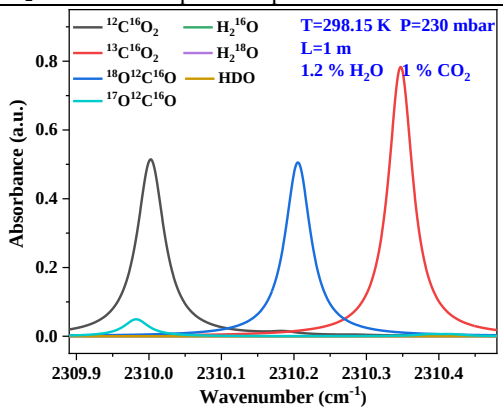

Figure 2. Simulated absorption lines of $^{13}C^{16}O_2$, $^{18}O^{12}C^{16}O$ and $^{12}C^{16}O_2$ in the wavenumber range of 2309.89cm^{-1}-2310.52cm^{-1}.

RESULTS AND DISCUSSION

Parameter Optimization. The key parameters used for the HPSDS-based CO_2 isotope detection system, i.e. pressure, modulation frequency and modulation depth are optimized. Considering the bandwidth of the used signal generator (the maximum is limited to 160 MHz) and the good separation of the absorption spectra of the three CO_2 isotopes ($^{13}C^{16}O_2$, $^{18}O^{12}C^{16}O$ and $^{12}C^{16}O_2$) at lower pressures, it is necessary to select the appropriate pressure and modulation frequency to obtain the best detection performance. A CO_2 sample of 3.33% prepared through the gas dilution system is filled into the HWG fiber through a pressure controller and a diaphragm pump. Four different modulation frequencies of 40 MHz, 80 MHz, 120 MHz and 160 MHz are selected and at each frequency 14 HPSDS signals are acquired at pressures ranging from 30 mbar to 500 mbar. Figure 3(a) shows the representative HPSDS signal spectrum of the three CO_2 isotopes at fixed pressure of 230 mbar and these four modulation frequencies. The peak-to-peak amplitude of the dispersion signal is generally used to provide direct measurement of concentration [43]. It is noted that the amplitude of the HPSDS signal in this paper refers to the peak-to-peak amplitude of the HPSDS signal. Among the three isotopes, the isotope $^{13}C^{16}O_2$ is selected as a representative to optimize the system parameters. Figure 3(b) shows the relationship between the amplitude of the HPSDS signal for $^{13}C^{16}O_2$ and pressure at different modulation frequencies.

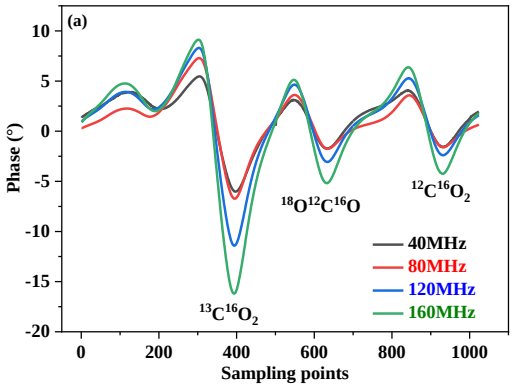

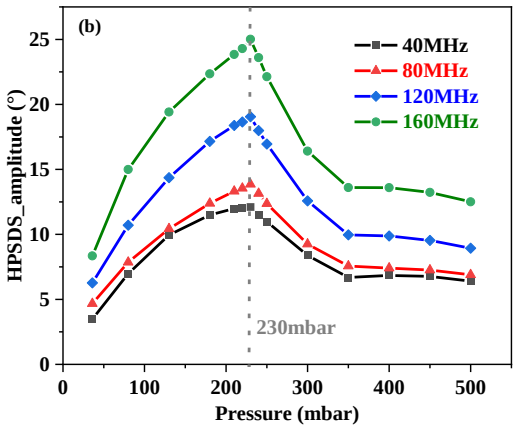

Figure 3. (a) HPSDS spectral signals of the three CO_2 isotopes at four modulation frequencies and the pressure of 230 mbar. (b) The relationship between the peak-to-peak amplitude of the HPSDS signals vs. pressure for 40 MHz, 80 MHz, 120 MHz and 160 MHz.

As seen in Figure 3(b), the HPSDS signal amplitude increases correspondingly with increasing pressure at low pressure due to the molecular absorption enhancement. At 160 MHz, 230 mbar, the HPSDS signal amplitude is maximized. Since the modulation frequency of the current setting is lower than the full width at half-maximum (FWHM) of the absorption line [31], the HPSDS signal amplitude decreases gradually when the pressure increases further. Therefore, we select 160MHz, 230mbar as the optimal setting for the current sensing system.

In the HPSDS technique, the amplitude of the modulation signal can have a significant effect on the HPSDS signal. Figure 4 records the variation of the $^{13}C^{16}O_2$ HPSDS signal amplitude for different modulated voltages. The modulated voltages is determined by the peak-to-peak voltage of the SG2, which can be up to 1 Vpp after the output of the power divider. It can be seen that the amplitude of the HPSDS signal for $^{13}C^{16}O_2$ is maximized at 1 Vpp, and its growth trend does not saturate at the current system setting. We thus select 1 Vpp as the optimal amplitude of the modulated signal for the current sensing system.

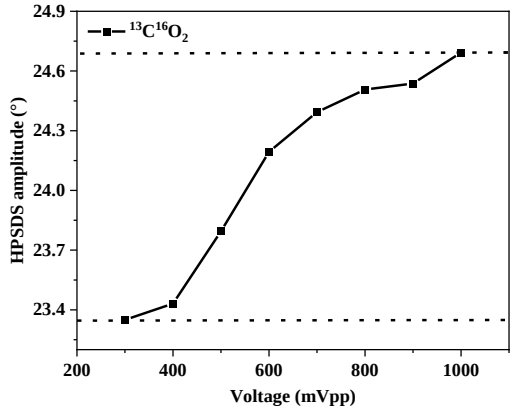

Figure 4. Variation of the HPSDS signal amplitudes for different modulation voltages.

System performance of the developed HPSDS. In the subsequent experimental part, the experimental conditions of the developed HPSDS are as the follows: pressure at 230 mbar,

modulation frequency of 160 MHz and modulation amplitude of 1 Vpp. The performance of the developed HWG-based CO_2 isotope HPSDS detection system is evaluated in terms of linearity, long-term stability and sensitivity. To test the linearity, seven samples of CO_2 gas with different standard concentrations (0.97%, 1.45%, 2.40%, 3.33%, 4.25%, 5.14% and 6.02%) are prepared using a gas dilution system to fill the HWG fiber. The relationship between the measured HPSDS signal amplitudes and concentrations for the three isotopes is shown in Figure 5, based on the natural abundance of $^{13}C^{16}O_2$, $^{18}O^{12}C^{16}O$ and $^{12}C^{16}O_2$. The result at each concentration is the average of 500 sampling points. The R^2 is 0.99974, 0.99864 and 0.99491, respectively, which indicates the excellent linear response of the system. The fitted curve is used as a calibration function to determine the CO_2 isotope concentration.

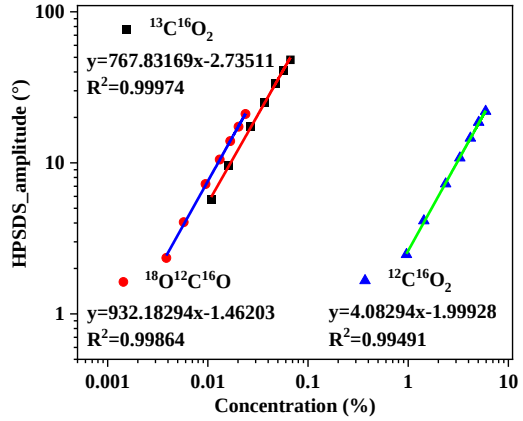

Figure 5. Amplitude of HPSDS versus CO_2 isotope concentration.

To characterize the long-term stability of the CO_2 isotope detection system, a 3.20% CO_2 gas sample was measured continuously over 130 minutes. The developed detection system has a high noise level, therefore, to obtain a higher signal-to-noise ratio and an appropriate temporal resolution, spectral data were averaged in a finite number of times resulting in the collection of a dispersion spectrum every 2.84s. Figure 6 displays the time series of the three CO_2 isotopes' concentrations and histogram plots of the concentration distribution for the measured CO_2 isotopes. The corresponding average concentration values for $^{13}C^{16}O_2$, $^{18}O^{12}C^{16}O$ and $^{12}C^{16}O_2$ are 370.55 ± 2.35 ppm, 128.37 ± 0.98 ppm, and 31239.53 ± 191.96 ppm, with relative uncertainties of 0.6, 0.7, and 0.6%, respectively. This indicates the better stability of the system. Furthermore, it can be observed that the histograms of the concentration distribution for the three isotopes are not well fitted by the Gaussian function. Since the dispersion information measured by HPSDS is encoded in the phase of the received light, the optical negative feedback of the HWG and the edge noise of the optical coupling may also introduce random phase variations and be added to the dispersion phase, resulting in an increase in the noise level [49]. Allan variance is performed on the long-term concentration fluctuation data in Figure 6 to assess the detection limits of the three CO_2 isotopes. At the integration time of 218 s, $^{13}C^{16}O_2$, $^{18}O^{12}C^{16}O$ and $^{12}C^{16}O_2$ are 0.29 ppm, 65.78 ppb and 14.65 ppm, respectively.

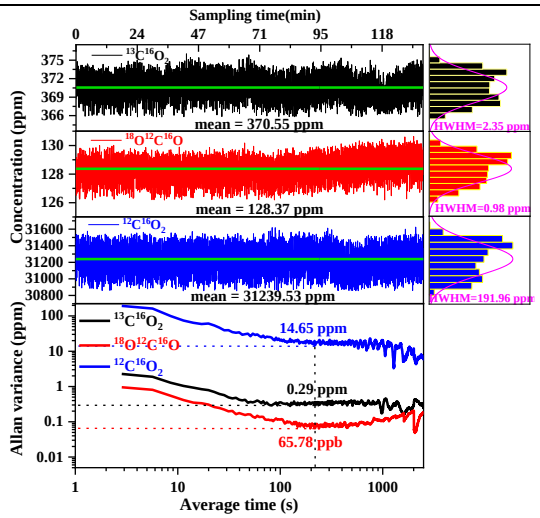

Figure 6. Long-term measurement results for the HWG-based experimental HPSDS setup and the corresponding Allan variance plots.

$\delta^{13}C$ and $\delta^{18}O$ were calculated by Eq. (3) and Eq. (4) for the data in Fig. 6 using the calibration gas. The averaged values of $\delta^{13}C$ and $\delta^{18}O$ are −21.15 ‰ and −28.63‰ respectively, and the 1σ precisions are 9.26 ‰ and 9.69 ‰, respectively. The Allan variance was used to determine the precision of $\delta^{13}C$ and $\delta^{18}O$, and the results are shown in Figure 7. The precision of $\delta^{13}C$ and $\delta^{18}O$ can reach 0.89 ‰ and 0.88 ‰, respectively, which corresponds to an integration time of 167 s.

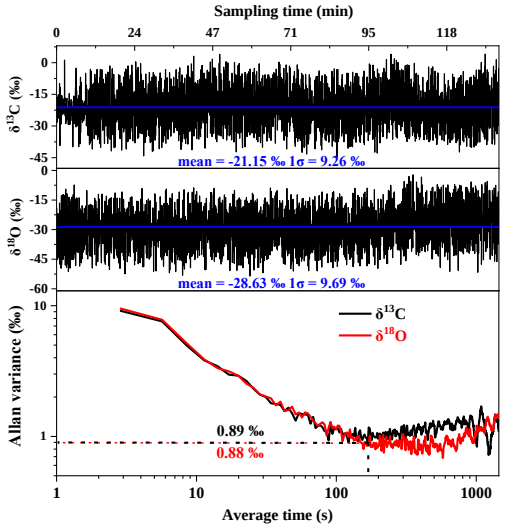

Figure 7. Allan variance of calculated $\delta^{13}C$ and $\delta^{18}O$.

In the Supporting Information, we provide an experimental comparison of HPSDS and WMS-2f to assess their linear dynamic range and long-term stability. A much wider linear dynamic range and good long term stability of present sensor is well compared to conventional absorption detection based sensors.

Table 1 summarized the carbon and oxygen isotope ratios measurement results of various modern laser absorption spectrometers reported in the literature and the corresponding key experimental parameters. Current laser absorption spectrometers have demonstrated excellent precision, typically between 0.01‰ and 0.1‰, through multi-channel or cavity-enhanced gas cells [17-19, 54]. However, these well-validated methods do not

allow for rapid updating of samples in the gas chamber and require large sample volume, which cannot meet the needs of micro-analysis in geochemistry, ecology and medical diagnostics, where large amount of samples are usually rarely available. HWG typical has very small volume, which can be easily filled with trace sample analyses. In this work, we apply HPSDS to the HWG gas sensor to obtain a precision of 0.88% for $\delta^{13}C$ and $\delta^{18}O$, which is in the same order of magnitude as other HWG-based gas sensor. The determined precision is sufficient to meet application scenarios in geochemical and medical diagnostic.

Table 1. Summary of carbon and oxygen isotope ratios measured by modern laser absorption spectrometer and the corresponding system parameters.

Ref.	λ (μm)	Method	Cell	L_{eff} (m)	Vol. (mL)	C (ppm)	Precision (‰) $\delta^{13}C$	Precision (‰) $\delta^{18}O$
[17]	4.32	TDLAS	MPC	36	-	400	<0.01	<0.05
[50]	2.00	TDLAS	MPC	29.9	900	346.6	0.24	-
[11]	4.32	TDLAS	Single	0.54	205	50000	0.12	-
[52]	4.31	TDLAS	MPC	6.3	15	600	0.3	-
[54]	4.3	OA-ICOS	Cavity	>200	-	~1500	0.07	0.07
[53]	4.35	TDLAS	MPC	41	-	0.2	0.61	-
[51]	4.33	TDLAS	Single	0.15	<5	50000	0.12	0.18
[19]	4.35	TDLAS	MPC	3	250	7000	<0.01	-
[6]	2.05	OA-ICOS	Cavity	-	-	50000	-	0.11
[18]	4.3	TDLAS	MPC	24	-	500	0.01	-
[49]	4.34	TDLAS	HWG	0.8	0.63	~400	~1	-
[25]	2.73	TDLAS	HWG	5	3.9	47000	0.72	0.72
[23]	4.35	TDLAS	iHWG	0.075	0.31	30000	1.3	-
Our	4.32	HPSDS	HWG	1	0.78	32000	0.89	0.88

Measurement of human breathing gas. Figure 8 shows the mean values and error bars of $\delta^{13}C$ and $\delta^{18}O$ determined from five human exhaled breath samples under the same experimental conditions. Three gas sampling bags were prepared including calibrated CO_2 sample, high purity N_2, and breathing gases. Before measuring breathing gases, a calibrated CO_2 sample was passed into the HWG to calibrate the spectrometer. During each measurement, the breathing gas samples were purged with dry N_2 for a period of time before being re-injected. The data set shown by each error bar records the time series of sample determinations after averaging. The error bars of $\delta^{13}C$ and $\delta^{18}O$ for each measurement are typically better than 1.2 ‰. The mean values of the five measurements for $\delta^{13}C$ and $\delta^{18}O$ are -29.17 ± 0.75 ‰ and -16.41 ± 0.53 ‰, respectively.

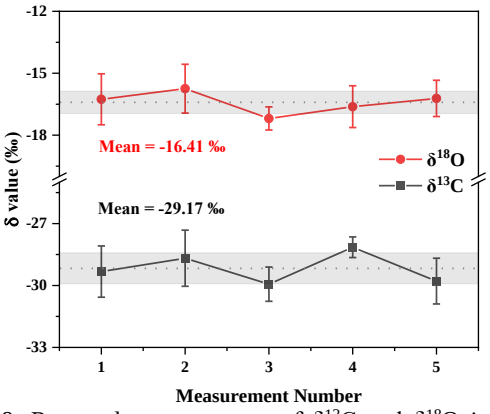

Figure 8. Repeated measurements of $\delta^{13}C$ and $\delta^{18}O$ in human breathing gas.

CONCLUSIONS

We demonstrate, for the first time, the measurement of CO_2 isotope ratios using mid-infrared HPSDS using an HWG fiber. A 4.329 μm ICL is used as the light source, targeting three CO_2 isotopes ($^{13}C^{16}O_2$, $^{18}O^{12}C^{16}O$ and $^{12}C^{16}O_2$). The system performance at different pressures, modulation frequencies, and modulation depths is studied and discussed to optimize the system parameter settings. At a pressure of 230 mbar, a modulation frequency of 160 MHz and modulation amplitude of 1 Vpp, the HPSDS system exhibits excellent linear response in the concentration range of 0.97 % to 6.02 % and achieves long-term stability of CO_2 isotope detection by measuring CO_2 at 3.20 % for more than 130 minutes. Measured mean values of $^{13}C^{16}O_2$, $^{18}O^{12}C^{16}O$ and $^{12}C^{16}O_2$ are 370.55 ppm, 128.37 ppm, and 31239.53 ppm, with relative uncertainties of 0.6, 0.7, and 0.6 %, respectively. For 1m HWG fiber, Allan variance analysis shows that the detection limits of $^{13}C^{16}O_2$, $^{18}O^{12}C^{16}O$ and $^{12}C^{16}O_2$ are 0.29 ppm, 65.78 ppb and 14.65 ppm, respectively, in an integration time of 218s. The measurement precisions of $\delta^{13}C$ and $\delta^{18}O$ are 0.89 ‰ and 0.88 ‰ at an integration time of 167s, respectively. We investigated the repeatability for the determination of $\delta^{13}C$ and $\delta^{18}O$ in human breathing gas, and obtained $\delta^{13}C$ and $\delta^{18}O$ values of (-29.17 ± 0.75) ‰ and (-16.41 ± 0.53) ‰, respectively. Additionally, compared to WMS-2f, the developed HPSDS exhibits a greater linear dynamic range and stability, and the precision of both $\delta^{13}C$ and $\delta^{18}O$ is improved at least 2 times. This demonstrates the positive impact of HPSDS on the performance of the spectroscopic system and clearly indicates the potential of the proposed sensing system for respiration analysis in medical diagnostics through appropriate sensor configurations, combined with a well-developed HWG and HPSDS technology with a large dynamic range.

ASSOCIATED CONTENT

Supporting Information

Additional experimental details and results for the comparison of HPSDS and WMS-2f in dynamic range and long-term stability.

AUTHOR INFORMATION

Corresponding Author

Tao Wu - *Key Laboratory of Nondestructive Test (Ministry of Education), Nanchang Hangkong University, Nanchang, 330063, China*; E-mail: wutccnu@nchu.edu.cn

Authors

Haojie Zhang, Chenwen Ye, Mengyu Wang, Xingdao He - *Key Laboratory of Nondestructive Test (Ministry of Education), Nanchang Hangkong University, Nanchang, 330063, China*

Qiang Wu - *Department of Mathematics, Physics and Electrical Engineering, Northumbria University, Newcastle upon Tyne, NE1 8ST, UK*

Weidong Chen - *Laboratoire de Physicochimie de l'Atmosphère, Université du Littoral Côte d'Opale 189A, Av. Maurice Schumann, Dunkerque 59140, France*

Notes

The authors declare no competing financial interest.

ACKNOWLEDGMENT

The authors acknowledge the support of the National Natural Science Foundation of China (Grant No. 42175130, 61965013), the Key Program of Natural Science Foundation of Jiangxi Province, China (No. 20232ACB202002) and Training Funding Project of High-Level and High-Skill Leading Talent of Jiangxi Province, China.

REFERENCES

(1) Mason, E.; Edmonds, M.; Turchyn, A. V. Remobilization of crustal carbon may dominate volcanic arc emissions. *Science* **2017**, *357*, 290-294.

(2) Boesch, H.; Liu, Y.; Tamminen, J.; Yang, D.; Palmer, P. I.; Lindqvist, H.; Cai, Z.; Che, K.; Noia, A. D.; Feng, L.; Hakkarainen, J.; Ialongo, I.; Kalaitzi, N.; Karppinen, T.; Kivi, R.; Kivimäki, E.; Parker, R. J.; Preval, S.; Wang, J.; Webb, A. J.; Yao L. and Chen H. Monitoring greenhouse gases from space. *Remote Sens*. **2021**, *13*, 2700.

(3) Zare, R. N.; Kuramoto, D. S.; Haase, C.; Tan, S. M.; Crosson, E. R. and Saad N. M. R. High-precision optical measurements of $^{13}C/^{12}C$ isotope ratios in organic compounds at natural abundance. *Proc. Natl. Acad. Sci.* **2009**, *106*, 10928-10932.

(4) Geldern, R. van; Nowak, M. E.; Zimmer, M.; Szizybalski, A.; Myrttinen, A.; Barth, J. A. C.; Jost, H. J. Field-based stable isotope analysis of carbon dioxide by mid-infrared laser spectroscopy for carbon capture and storage monitoring. *Anal. Chem.* **2014**, *86*, 12191-12198.

(5) Castrillo, A.; Casa, G.; Van Burgel, M.; Tedesco, D.; Gianfrani, L. First field determination of the $^{13}C/^{12}C$ isotope ratio in volcanic CO_2 by diode-laser spectrometry. *Opt Express* **2004**, *12*, 6515-23.

(6) Yakir, D.; Sternberg, L.S.L.The use of stable isotopes to study ecosystem gas exchange, *Oecologia* **2000**, *12*, 297-311.

(7) Cao, W.; Duan, Y. Breath analysis: potential for clinical diagnosis and exposure assessment. *Clin. chem*. **2006**, *52*, 800-811.

(8) Ghosh, C.; Mandal, S.; Banik, G. D. Targeting erythrocyte carbonic anhydrase and 18O-isotope of breath CO_2 for sorting out type 1 and type 2 diabetes. *Scientific Reports*, **2016**, *6*, 35836.

(9) Coelho, L. G. V.; Reber, M.; Passos, M. C. F. Application of isotope-selective non-dispersive infrared spectrometry for the evaluation of the 13C-urea breath test: comparison with three concordant methods. *Med. Biol. Res*, **1999**, *32*, 1493-1497.

(10) Som, S.; De, A.; Banik, G. D.; Maity, A.; Ghosh, C.; Pal, M.; Daschakraborty, S. B.; Chaudhuri, S.; Jana S; Pradhan, M. Mechanisms linking metabolism of Helicobacter pylori to ^{18}O and ^{13}C-isotopes of human breath CO_2. *Sci. Rep*. **2015**, *5*, 10936.

(11) Kasyutich, V. L.; Martin, P. A. $^{13}CO_2/^{12}CO_2$ isotopic ratio measurements with a continuous-wave quantum cascade laser in exhaled breath. *Infrared Physics & Technology*, **2012**, *55*, 60-66.

(12) Becker, J. S. Recent developments in isotope analysis by advanced mass spectrometric techniques plenary lecture. *J. Anal. At. Spectrom.* **2005**, *20*, 1173-1184.

(13) Vogt, J. A.; Wachter, U.; Mehring, J.; Radermacher, P.; Georgieff, M.; Fischer, H.; Hölscher, U.; Moede, M.; Fabinski, W. Adaptation of the NDIR technology to $^{13}CO_2$ breath tests under increased inspiratory O_2 concentrations. *J. Appl. Physiol*. **2009**, *107*, 302-307.

(14) Sakai, S.; Otsuka, T.; Matsuda, S. Subnanomolar sensitive stable isotopic determination in CO_2 by tunable infrared laser absorption spectroscopy. *Anal. Chem*. **2022**, *94*, 6446-6450.

(15) Hare, V J.; Dyroff, C.; Nelson, D. D. High-Precision Triple Oxygen Isotope Analysis of Carbon Dioxide by Tunable Infrared Laser Absorption Spectroscopy. *Anal. Chem*, **2022**, *94*, 16023-16032.

(16) Nataraj, A.; Tuzson, B.; Gianella, M. Position-Specific Isotope Analysis of Propane by Mid-IR Laser Absorption Spectroscopy. *Anal. Chem*, **2023**, *95*, 5354-5361.

(17) Steur, P. M.; Scheeren, H. A.; Nelson, D. D. Simultaneous measurement of $\delta^{13}C$, $\delta^{18}O$ and $\delta^{17}O$ of atmospheric CO_2-performance assessment of a dual-laser absorption spectrometer. *Atmospheric Measurement Techniques*, **2021**, *14*, 4279-4304.

(18) Zhang, H.; Wen, M.; Li, Y. High-precision $^{13}CO_2/^{12}CO_2$ isotopic ratio measurement using tunable diode laser absorption spectroscopy at 4.3 μm for deep-sea natural gas hydrate exploration. *Applied Science*s, **2019**, *9*, 3444.

(19) Li, G.; Zhang, X.; Zhang, Z. A mid-infrared exhaled carbon dioxide isotope detection system based on 4.35 μm quantum cascade laser. *Optics & Laser Technology*, **2022**, *152*, 108117.

(20) Kasyutich, V. L.; Martin, P. A.; & Holdsworth, R. J. An off-axis cavity-enhanced absorption spectrometer at 1605 nm for the $^{12}CO_2/^{13}CO_2$ measurement. *Appl. Phys. B* **2006**, *85*, 413-420.

(21) Crosson, E. R.; Ricci, K. N.; Richman, B. A.; Chilese, F. C.; Owano, T. G.; Provencal, R. A.; Todd, M. W.; Glasser J.; Kachanov, A. A.; Paldus, B. A.; Spence, T. G; Zare, R. N. Stable isotope ratios using cavity ring-down spectroscopy: determination of $^{13}C/^{12}C$ for carbon dioxide in human breath. *Anal. Chem.* **2002**, *74*, 2003-2007.

(22) Ding, W.; Sun, L.; Yi, L.; Zhang, E. 'Baseline-offset'scheme for a methane remote sensor based on wavelength modulation spectroscopy. *Meas. Sci. Technol*. **2016**, *27*, 085202.

(23) Tütüncü, E.; Nägele, M.; Becker, S. Advanced photonic sensors based on interband cascade lasers for real-time mouse breath analysis. *ACS sensors*, **2018**, *3*, 1743-1749.

(24) Zhou, T.; Wu, T.; Wu, Q. Real-time monitoring of ^{13}C-and ^{18}O-isotopes of human breath CO_2 using a mid-infrared hollow waveguide gas sensor. *Anal. Chem*, **2020**, *92*, 12943-12949.

(25) Liu, Y.; Wu, T.; Wu, Q.; Chen, W.; Ye, C.; Wang, M.; He X. A Laser-Locked Hollow Waveguide Gas Sensor for Simultaneous Measurements of CO_2 Isotopologues with High Accuracy, Precision, and Sensitivity. *Anal. Chem.* **2021**, *93*, 15468-15473.

(26) Chakraborty, A. L.; Ruxton, K.; Johnstone, W.; Lengden, M.; Duffin, K. Elimination of residual amplitude modulation in tunable diode laser wavelength modulation spectroscopy using an optical fiber delay line. *Opt. Express* **2009**, *17*, 9602-9607.

(27) Nikodem, M.; Wysocki, G. Chirped laser dispersion spectroscopy for remote open-path trace-gas sensing. *Sensors* **2012**, *12*, 16466-16481.

(28) Janik, G. R.; Carlisle, C. B.; Gallagher, T. F. Two-tone frequency-modulation spectroscopy. *J. Opt. Soc. Am. B* **1986**, *3*, 1070-1074.
(29) Rieker, G. B.; Giorgetta, F. R.; Swann, W. C.; Kofler, J.; Zolot, A. M.; Sinclair, L. C.; Baumann, E.; Cromer, C.; Petron, G.; Sweeney, C.; Tans, P. P.; Coddington, I.; Newbury, N. R. Frequency-comb-based remote sensing of greenhouse gases over kilometer air paths. *Optica* **2014**, *1*, 290-298.
(30)Wysocki, G.; Weidmann, D. Molecular dispersion spectroscopy for chemical sensing using chirped mid- infrared quantum cascade laser. *Opt. Express* **2010**, *18*, 26123-26140.
(31) Martín-Mateos, P.; Acedo, P. Heterodyne phase-sensitive detection for calibration-free molecular dispersion spectroscopy. *Opt. Express*, **2014**, *22*, 15143-15153.
(32) Jaworski, P.; Krzempek, K.; Bojęś, P.; Wu, D.; Yu, F. Mid-IR antiresonant hollow-core fiber based chirped laser dispersion spectroscopy of ethane with parts per trillion sensitivity. *Opt. Laser Technol.* **2022**, *156*, 108539.
(33) Nikodem M.; Wysocki, G. Measuring optically thick molecular samples using chirped laser dispersion spectroscopy. *Opt. Lett.* **2013**, *38*, 3834-3837.
(34) Ding, W.; Sun, L. Phase sensitive chirped laser dispersion spectroscopy under high absorbance conditions. *Acta Phys. Sin*. **2017**, *66*, 120601.
(35) Ding, W.; Sun, L.; Yi, L.; Ming, X. Dual-sideband heterodyne of dispersion spectroscopy based on phase-sensitive detection. *Appl. Opt*. **2016**, *55*, 8698–8704.
(36) Zou, M.; Sun, L.; Li, S. Simultaneous measurement of gas absorption and path length based on the dual-sideband heterodyne phase-sensitive detection of dispersion spectroscopy. *Opt. Express* **2021**, *29*, 11683-11692.
(37) Wang, R; Pang, Y; Tang, X. Simultaneous measurement of temperature and water concentration using a novel laser dispersion spectrum extraction method immune to carrier phase variation. *Opt. Laser Eng.* **2023**, 164: 107497.
(38) Cooper, D. E.; Martinelli, R. U.; Carlisle, C. B.; Riris, H.; Bour, D. B.; Menna, R. J. Measurement of $^{12}CO_2/^{13}CO_2$ ratios for medical diagnostics with 1.6-μm distributed-feedback semiconductor diode lasers. *Appl. Opt*. **1993**, *32*, 6727–6731.
(39) Andreev, S. N.; Mironchuk, E. S.; Nikolaev, I. V.; Ochkin, V. N.; Spiridonov, M. V.; Tskhai, S. N. High precision measurements of the $^{13}CO_2/^{12}CO_2$ isotope ratio at atmospheric pressure in human breath using a 2μm diode laser. *Appl. Phys. B* **2011**, *104*, 73–79.
(40) Kasyutich, V. L.; Martin, P. A. $^{13}CO_2/^{12}CO_2$ isotopic ratio measurements with a continuous-wave quantum cascade laser in exhaled breath. *Infrared Phys.Techn.* **2012**, *55*, 60–66.
(41) Martín-Mateos, P.; Hayden, J.; Acedo, P.; Lendl, B. Heterodyne phase-sensitive dispersion spectroscopy in the mid-infrared with a quantum cascade laser. *Anal. Chem.* **2017**, *89*, 5916-5922.
(42) Ma, L.; Wang, Z.; Cheong, K.; Ning, H.; Ren, W. Mid-infrared heterodyne phase-sensitive dispersion spectroscopy in flame measurements. *P. Combust. Inst.* **2019**, *37*, 1329-1336.
(43) Wang, Z.; Cheong, K.; Li, M.; Wang, Q.; Ren, W. Theoretical and Experimental Study of Heterodyne Phase-Sensitive Dispersion Spectroscopy with an Injection-Current-Modulated Quantum Cascade Laser. *Sensors* **2020**, *20*, 6176.
(44) Tütüncü, E.; Kokoric, V.; Wilk, A.; Seichter, F.; Schmid, M.; Hunt, W. E.; Manuel, A. M.; Mirkarimi, P.; Alameda, J. B.; Carter, J. C.; Mizaikoff B. Fiber-coupled substrate-integrated hollow waveguides: an innovative approach to mid-infrared remote gas sensors. *ACS sens*. **2017**, *2*, 1287-1293.
(45) Toll, J. S. Causality and the dispersion relation: logical foundations. *Phys. Rev.* **1956**, *104*, 1760-1770.
(46) Hangauer, A.; Spinner, G.; Nikodem, M.; Wysocki, G. High frequency modulation capabilities and quasi single-sideband emission from a quantum cascade laser. *Opt. Express* **2014**, *22*, 23439-23455.
(47) Griffith, D. W. T. Calibration of isotopologue-specific optical trace gas analysers: a practical guide. *Atmospheric Measurement Techniqu*es, **2018**, *11*, 6189-6201.
(48) Gordon, I. E.; Rothman, L. S.; Hargreaves, R. J.; Hashemi, R.; Karlovets, E. V.; Skinner, F. M.; Conway, E. K.; Hill, C.; Kochanov, R. V.; Tan, Y.; Wcislo, P.; Finenko, A. A.; Nelson, K.; Bernath, P. F.; Birk, M.; Boudon, V.; Campargue, A.; Chance, K. V.; Coustenis, A.; Drouin, B. J.; Flaud, J.-M.; Gamache, R. R.; Hodges, J. T.; Jacquemart, D.; Mlawer, E. J.; Nikitin, A. V.; Perevalov, V. I.; Rotger, M.; Tennyson, J.; Toon, G. C.; Tran, H.; Tyuterev, V. G.; Adkins, E. M.; Baker, A.; Barbe, A.; Cane, E.; Csaszar, A. G.; Dudaryonok, A.; Egorov, O.; Fleisher, A. J.; Fleurbaey, H.; Foltynowicz, A.; Furtenbacher, T.; Harrison, J. J.; Hartmann, J.-M.; Horneman, V.-M.; Huang, X.; Karman, T.; Karns, J.; Kassi, S.; Kleiner, I.; Kofman, V.; Kwabia-Tchana, F.; Lavrentieva, N. N.; Lee, T. J.; Long, D. A.; Lukashevskaya, A. A.; Lyulin, O. M.; Makhnev, V. Yu.; Matt, W.; Massie, S. T.; Melosso, M.; Mikhailenko, S. N.; Mondelain, D.; Muller, H. S. P.; Naumenko, O. V.; Perrin, A.; Polyansky, O. L.; Raddaoui, E.; Raston, P. L.; Reed, Z. D.; Rey, M.; Richard, C.; Tobias, R.; Sadiek, I.; Schwenke, D. W.; Starikova, E.; Sung, K.; Tamassia, F.; Tashkun, S. A.; Vander Auwera, J.; Vasilenko, I. A.; Vigasin, A. A.; Villanueva, G. L.; Vispoel, B.; Wagner, G.; Yachmenev, A.; Yurchenko, S. N. The HITRAN2020 molecular spectroscopic database. *J. Quant. Spectrosc. Radiat. Transfer* **2022**, *277*, 107949.
(49) Kelly, J. F.; Sams, R. L.; Blake, T. A. A capillary absorption spectrometer for stable carbon isotope ratio ($^{13}C/^{12}C$) analysis in very small samples. *Rev. Sci. Instrum*, **2012**, *83*, 023101.
(50) Tanaka, K.; Tonokura, K. Sensitive measurements of stable carbon isotopes of CO_2 with wavelength modulation spectroscopy near 2 μm. *Appl. Phys. B*, **2011**, *105*, 463-469.
(51) Shao, L.; Mei, J.; Chen, J.; Simultaneous Sensitive Determination of $\delta^{13}C$, $\delta^{18}O$, and $\delta^{17}O$ in Human Breath CO_2 Based on ICL Direct Absorption Spectroscopy. *Sensors*, **2022**, *22*, 1527.
(52) Chen, H.; Chen, C.; Dong, W. Mid-infrared dissolved CO_2 measurement system using the ultra-compact multipass cell. *Microwave and Optical Technology Letters*, **2023**, 65, 1319-1323.
(53) Li, G.; Zhao, H.; Song, Y.; Mid-infrared carbon isotope spectrum logging system combined with a thermostat of optical subsystem for high-precision detection of isotope ratio. *Spectrochimica Acta Part A: Molecular and Biomolecular Spectroscopy*, **2023,** 123051.
(54) Beinlich, A.; Barker, S. L. L.; Dipple, G. M. Stable isotope ($\delta^{13}C$, $\delta^{18}O$) analysis of sulfide-bearing carbonate samples using laser absorption spectrometry. *Economic Geology*, **2017**, *112*, 693-700.

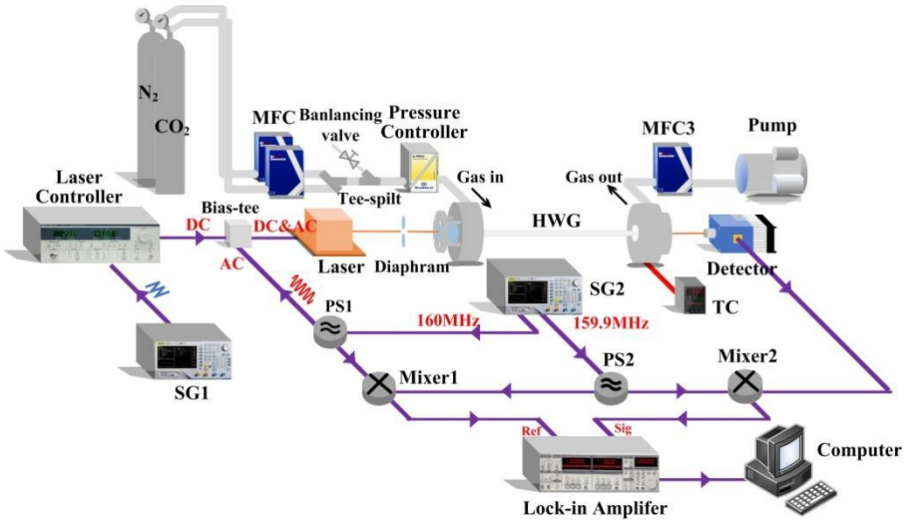

For Table of Contents Only